


RESEARCH ARTICLE

Open Access



Highly fluorescent hydroxyl groups functionalized graphitic carbon nitride for ultrasensitive and selective determination of mercury ions in water and fish samples

Y. G. Abou El-Reash^{1,2}, Eslam A. Ghaith¹, Osama El-Awady¹, Faisal K. Algethami², Haiqing Lin³, Ehab A. Abdelrahman^{2,4} and Fathi S. Awad^{1*} 

Abstract

Heavy metal ion pollution is always a serious problem worldwide. Therefore, monitoring heavy metal ions in environmental water is a crucial and difficult step to ensure the safety of people and the environment. A mercury ion (Hg^{2+}) fluorescence probe with excellent sensitivity and selectivity is described here. The functionalized graphitic carbon nitride nanosheets (T/G- C_3N_4) fluorescence probe was fabricated using melamine as a precursor by the pyrolysis technique, followed by a rapid KOH heat treatment method for 2 min. The chemical structure and morphology of the T/G- C_3N_4 probe were characterized using multiple analytical techniques including UV-Vis, SEM, XPS, XRD, and fluorometer spectroscopy. Geometry optimization of T/G- C_3N_4 as a modified probe was performed to assess its stability and interaction ability with Hg(II) via using the density function approach. The T/G- C_3N_4 probe showed a linear response based on quenching over the range 0– 1.25×10^3 nM Hg(II); the detection limit was 27 nM. The remarkable sensitivity of T/G- C_3N_4 towards the Hg^{2+} ions was explained by the intense coordination and fast chelation kinetics of Hg^{2+} with the NH_2 , CN, C=N, and OH groups of T/G- C_3N_4 nanoprobe. The T/G- C_3N_4 probe demonstrates exceptional selectivity for Hg^{2+} ions among other metal ions including (Na^+ , Ag^+ , Mg^{2+} , Fe^{2+} , Fe^{3+} , Co^{2+} , Ni^{2+} , Cd^{2+} , K^+ , Ca^{2+} , Cu^{2+} , Pb^{2+} , Mn^{2+} and Hg^{2+}) and over a broad pH range (6–10), together with remarkable long-term fluorescence stability in water (> 30 days) and minimal toxicity. T/G- C_3N_4 was used to detect and quantify Hg^{2+} ions in tuna and mackerel fish and the results compared to ICP-AES. The results obtained offer a new simple and green technique for the design of multifunctional fluorescent probe appropriate for environmental applications.

Keywords G- C_3N_4 , Functionalization, Fluorescent sensor, Hg^{2+} sensor

*Correspondence:

Fathi S. Awad

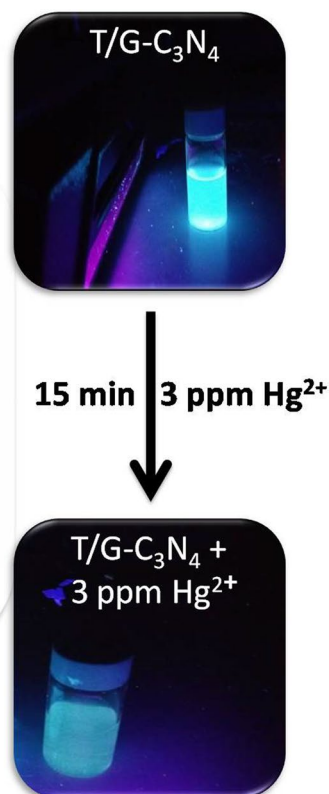
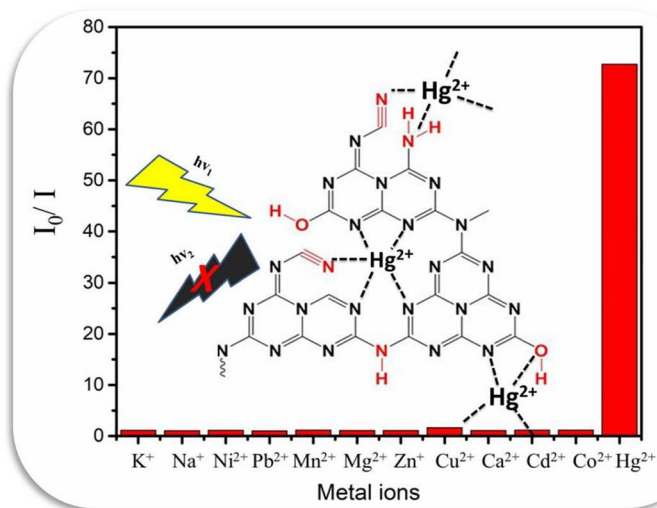
fathyawad949@yahoo.com; fathysamy@mans.edu.eg

Full list of author information is available at the end of the article



© The Author(s) 2023. **Open Access** This article is licensed under a Creative Commons Attribution 4.0 International License, which permits use, sharing, adaptation, distribution and reproduction in any medium or format, as long as you give appropriate credit to the original author(s) and the source, provide a link to the Creative Commons licence, and indicate if changes were made. The images or other third party material in this article are included in the article's Creative Commons licence, unless indicated otherwise in a credit line to the material. If material is not included in the article's Creative Commons licence and your intended use is not permitted by statutory regulation or exceeds the permitted use, you will need to obtain permission directly from the copyright holder. To view a copy of this licence, visit <http://creativecommons.org/licenses/by/4.0/>.

Graphical Abstract

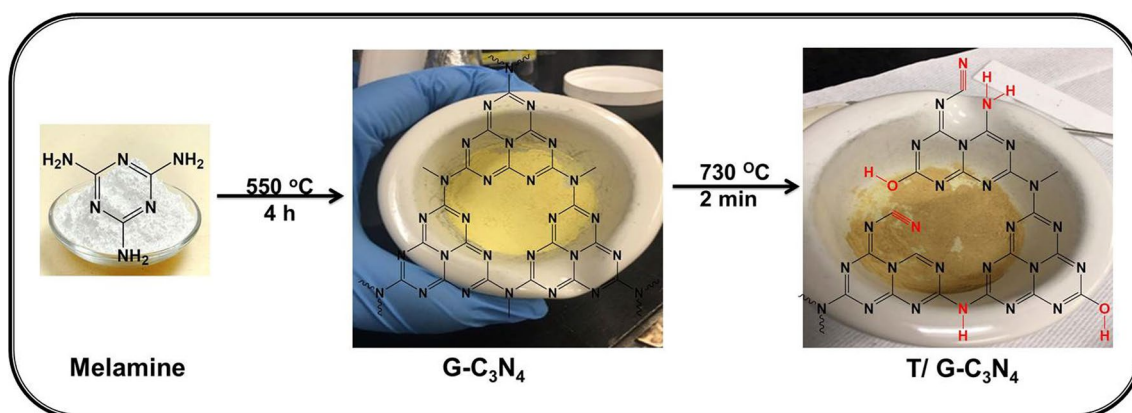


Introduction

In recent years, the World Health Organization (WHO) and the United States Environmental Protection Agency (US EPA) have listed mercury as one of the top public health societies. They have defined a series of levels in drinkable water (<10 nM), food (<50 nM) and atmosphere (<4 nM) (Awad et al. 2017; Pica 2021; Premkumar et al. 2018). Mercury contamination lead to a destruction of the biological system and became a significant danger to the environment and human because it is more poisonous than its lethal dose 50 (LD50) values might indicate (Wang et al. 2022). No doubt that mercury can be found naturally in the earth's from crust degassing of the Earth's crust through volcanic activities and weathering of rocks, but industrial and agricultural activities played a great role in raising its levels. Mercury exists in three inorganic forms; elemental Hg (Hg⁰), oxidized Hg (Hg²⁺), and particle-bound Hg (Hg_p) (Krabbenhoft and Sunderland 2013), and enters human bodies through the food chain. Besides, normal bacterial makeup of the human body can change these inorganic forms to organic forms leading to severe physiological impacts on the nervous

system, heart, kidneys, lungs, and immune systems (Anderson et al. 2006; Mortazavi et al. 2016). Mercury has non-biodegradation features, thus, it is of great significance to design a harmless, efficient and inexpensive Hg²⁺ testing material for detection and quantification of Hg²⁺ levels in different environmental or food samples.

To Date, miscellaneous techniques have been used for detecting Hg²⁺ levels in numerous samples, including spectrophotometric method using dithizone (Wang et al. 2018a, 2018b), cold vapor atomic absorption spectroscopy (Tian et al. 2019), inductively coupled plasma mass spectrometry (ICP-MS) (Sun et al. 2020) and electrochemical methods (Xie et al. 2022). Still, these techniques are usually complex, expensive for analysis and need high costs for maintenance, time-consuming and need complicated operation procedures, which limit their practical applications for routine analysis. In addition, since different samples and sources have various mercury content ranging from pM in gas to μM in polluted soil or water, most of the previous techniques have the disadvantages of non-wide linear range, therefore they cannot be used conveniently for environmental-monitoring applications



Scheme 1 General procedure for the preparation of T/G-C₃N₄ nanosheets

in diverse fields (Mortada et al. 2017; Romanovskiy et al. 2018). Accordingly, to overcome these difficulties and meet the requirement of food safety evaluation and environmental monitoring, many fluorescent nanomaterials such as carbon dots (Erdemir et al. 2022), luminescent molecular dyes (Rasheed et al. 2019), and luminescent metal nanocrystals (Zhang and Yu 2014) have been prepared and used to design fluorescent probes for Hg²⁺ detection. These fluorescent nanoprobe have the advantages of low cost, simple handling, high sensitivity, a fast response and low detection limit.

Nowadays, nanostructured graphitic carbon nitride (g-C₃N₄), which is a unique carbon based and chemically metal-free stable nanoarchitected material, has been widely used as a new fluorophore because; it owns several properties essential for sensing applications [e.g. good fluorescence stability over time, excellent fluorescence quenching phenomenon, high electron transfers characteristics, specificity, fast response, excellent thermochemical stability in both acidic and alkaline media and good water solubility (Li et al. 2014; Yin et al. 2021)]. Fundamentally, the exceptional fluorescence quenching capabilities of nano g-C₃N₄, were the reason behind applying many fluorescence probes in quantification and detection of various spices, such as glutathione (Xu et al. 2015), Cu²⁺ (Wang et al. 2018a, 2018b), Ag⁺ (Wang et al. 2018a, 2018b), Fe³⁺ (Cárdenas et al. 2021) and Hg²⁺ (Wang et al. 2017). In our study, a simple and cost effective method was used to prepare functionalized graphitic carbon nitride nanosheets (T/G-C₃N₄) by a rapid KOH heat treatment of G-C₃N₄ at 730 °C for 2 min. The obtained nano T/G-C₃N₄ exhibited a strong fluorescence intensity and an obvious linear quenching behavior by Hg²⁺. This quenching is a result of the interactions between Hg²⁺ and T/G-C₃N₄ nanoparticles, this interaction lead to an energy or an electron transfer from T/G-C₃N₄ surface to

the target metal ions. This developed analytical method offered a low detection limit for the determination of Hg²⁺ and was validated as their recovery study on applying for Hg(II) determination in some food samples.

Experimental

For more details on the chemicals and instruments, see Additional file 1: S1 and S2 respectively.

Synthesis of surface functionalized G-C₃N₄ (T/G-C₃N₄) nanosheets

The detailed method for the preparation of T/G-C₃N₄ is as follows. 3 g melamine powder was heated in a covered ceramic crucible for 1 h at 550 °C with a ramp rate of 3 °C/min and kept at this temperature for another 3 h in Argon environment. Then, KOH (0.15 g) was grinded very well with 0.5 g G-C₃N₄ in a ceramic mortar till the mixture become homogeneous, and then heated again at 730 °C for 2 min. The obtained product washed several times with deionized water until neutrality, then separated using central centrifuge at 6000 rpm for 6 min and dried in oven at 55 °C for 24 h. For a typical assay, a stock solution of 100 ppm T/G-C₃N₄ was prepared by dispersing 10 mg of the final dry powder in 100 mL of deionized distilled water under sonication for 6 h. The resulted solution was kept in a dark place. Scheme 1 depicts the general procedures for synthesizing T/G-C₃N₄ nanosheets.

Fluorescence sensing experiments

The influence of pH on T/G-C₃N₄ based fluorescence probe

The effect of pH on the fluorescence intensity of T/G-C₃N₄ was tested over a pH range 2–10. The pH for all studied solutions was adjusted before starting the experiments by adding 50 µL of prepared buffers (see Additional file 1: S1) to 300 µL of the T/G-C₃N₄ solution (10 mg/L) and then completed to a constant volume

(10 mL) with deionized water. The mixtures were vortexed for 5 min and after equilibration, the fluorescent intensity signals were collected at an excitation wavelength of 290 nm and excitation and emission slit widths of 5 nm. The fluorescence stability T/G-C₃N₄ probe over time was also investigated by detecting the change in the fluorescence intensity of 5 ppm T/G-C₃N₄ solution every week over 1 month.

Detection of different metal ions using T/G-C₃N₄

For Hg²⁺ detection, 50 µL of phosphate buffer (pH 6) and 300 µL of T/G-C₃N₄ suspension were added to 20 mL glass vial. Then the desired amount of mercury solution was added to make the final concentration of Hg(II) ranging from 0.1 to 3.0 ppm at constant volume of 10 mL. The mixtures were vortexed for 5 min and after equilibration, the change in the fluorescence intensity signals was detected at 290 nm.

The effect of interfering ions and matrix effect on the detection of Hg(II) was also conducted by adding 5 and 10 ppm of foreign metal ions to 3 ppm of Hg(II) solution and recording the change in the fluorescence intensity of T/G-C₃N₄.

Actual sample treatment

To assess the T/G-C₃N₄ as a probe for Hg²⁺ in real samples, tuna and mackerel fish were utilized. The samples were digested using concentrated HNO₃ (69–70%). 5 g of fish sample were dried at 70 °C for 5 h then crushed in a mortar for this purpose. The crushed sample was placed in an open beaker containing 95 mL of pure HNO₃ was added. The resulting mixture was heated and stirred for 1 h at 40 °C, and treatment continued for a further 3 h at 150 °C. The obtained mixture was allowed to cool to room temperature and then filtered to remove the undissolved tissues. The filtrate was utilized for the detection of the Hg²⁺ after the adjustment of the solution pH to 6 using NaOH (5 M).

Computational approach

Investigation of the geometry of synthesized T/G-C₃N₄ nanosheets can be achieved by using Gaussian 09 program package. As the quantum calculations and electronic properties of the prepared polymer were optimized in the presence of density functional theory (DFT) level, using the B3LYP/6-31 G (*d* to *p*) as the basis set (Abdallah et al. 2022). The optimum molecular geometry and electrostatic potential surface (ESP) of the synthesized T/G-C₃N₄ (represents as monomer) are shown in Fig. 1A and Additional file 1. Whereas, the electrostatic potential map illustrates distribution regions of electron deficiency and surplus electron density, and this explanation of increasing the fluorescence stability of the synthesized

T/G-C₃N₄ network due to having more nitrogen atoms acts as dentate atoms participating in coordination with Hg²⁺. Meanwhile, the presence of a huge hole between the poly functionalized dicyclic triazino rings (triazine with nitrogen atom ring junction) and tricyclic triazine ring indicates that probability of metal ions in this region increases extremely (Ramki et al. 2019).

In addition, energy calculations of frontier molecular orbitals (HOMO and LUMO) are essential parameters in quantum computational studies. Whereas, the HOMO level (π -donor) is for the most part allocated on the nitrogen atoms demonstrating the most electronegative charge density. On the other hand, LUMO level (π -acceptor) indicates the ability of a part of the molecule for receiving electrons. The energy gap ($E_{\text{HOMO}}-E_{\text{LUMO}}$) is a vital stability index in the investigation of the kinetic stability and chemical reactivity of the prepared polymer (Ghaith et al. 2020). Additionally, the low value of energy gap of the synthesized molecule (−3.173 eV) could be attributed to the incorporation of the triazine monomers into the poly functionalized conjugated polymer (Al-Assy et al. 2013), representative molecular orbitals (HOMO, LUMO and HOMO–LUMO) were presented in Fig. 1B.

Results and discussion

Characterization of G-C₃N₄ and T/G-C₃N₄ nanosheets

To prove the successful functionalization of G-C₃N₄ by KOH treatment at high temperature for 2 min, different analytical means were employed including FTIR, XRD, XPS, and SEM. FTIR spectra of G-C₃N₄ and T-G₃N₄ were collected and presented in Fig. 2. In the FTIR spectra of G-C₃N₄ and T-G₃N₄, the peaks that appeared in the range of 1100–1700 cm^{−1} are owing to the stretching of NCN heterocycles in the “melon” framework. The peak at 808 cm^{−1} is characteristic for the bending vibration of heptazine rings (Yang et al. 2019). These results revealed that the basic chemical structure of carbon nitride was kept constant after treatment with KOH at high temperature. Regarding to the FTIR spectrum of T-G C₃N₄, a new peak observed at 2169 cm^{−1} can be attributed to the stretching vibration of cyano groups (CN). This CN groups are formed as a results of the partial deprotonation of “melon” units by KOH treatment at high temperature (Zhang et al. 2018). Furthermore, an increase in the intensity of peaks at 3300–3550 cm^{−1}, that can be attributed to the stretching vibrations of OH groups and confirms that the number of OH groups increased on the surface of graphitic carbon nitride after KOH treatment. Whereas the decrease in the intensity of peaks located between 300 and 3300 cm^{−1}, attributed to the stretching vibration of NH₂ groups, indicates the partial deprotonation of NH₂ groups and the formation of NH_x groups (Zhang et al. 2018). These results clearly confirmed that

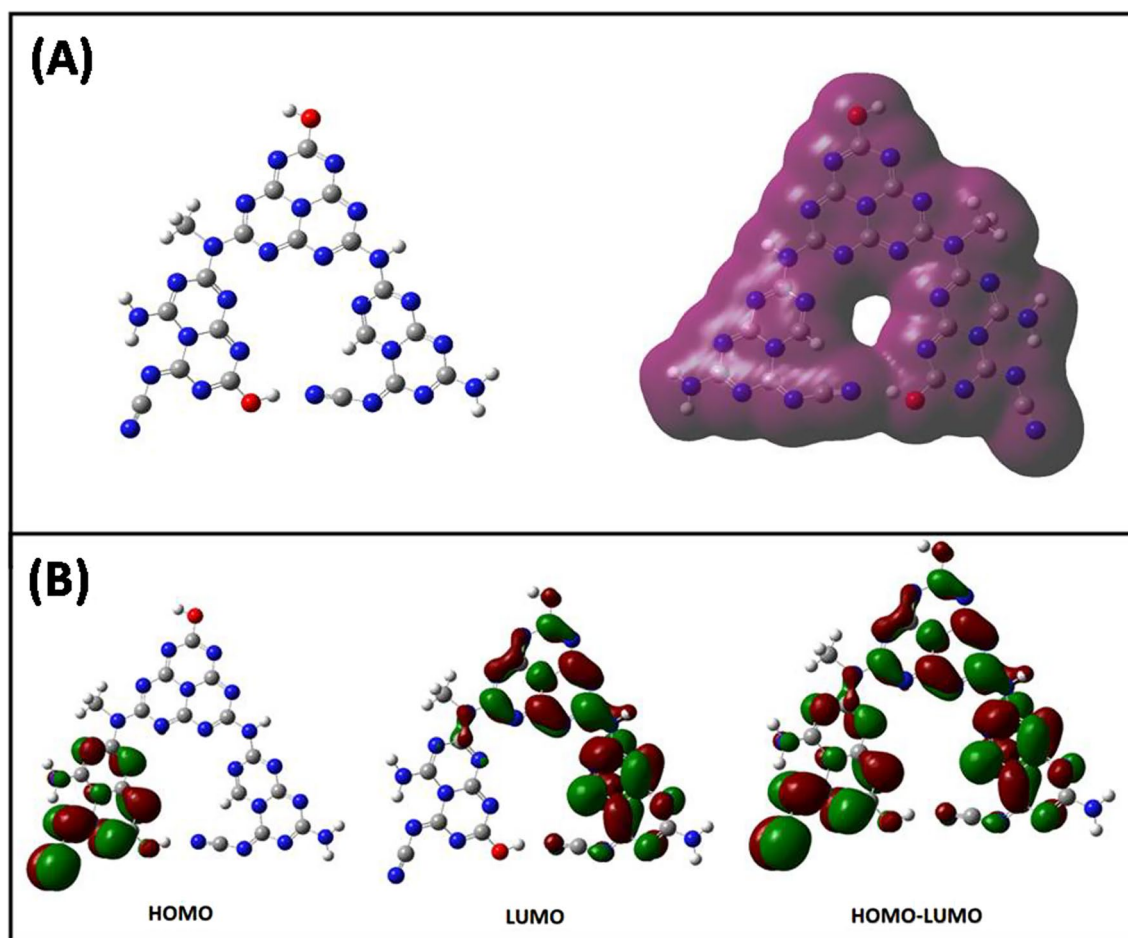


Fig. 1 **A** The optimum geometry and electrostatic potential map for structure. **B** Spatial distribution of calculated HOMO and LUMO orbitals of the synthesized T/G-C₃N₄ nanosheets

the surface of graphitic carbon nitride was modified by new functional groups (cyano, OH and NH_x groups) by KOH treatment at 730 °C. It should be noted that KOH has a melting point of roughly 360 °C. KOH after fusion can release the –OH during the fast heat treatment process at 730 °C, which may combine with amine groups to produce the cyano and NH_x groups. In addition, the released –OH can capture a proton from the tri-s-triazine units of G-C₃N₄, revealing more nitrogen sites and functionalizing the surface of G-C₃N₄ with amine and hydroxyl groups (Li et al. 2016).

The XRD pattern of G-C₃N₄ and KOH treated G-C₃N₄ at high temperature are shown in Additional file 1: Fig. S2. The native G-C₃N₄ showed two characteristic peaks. A strong diffraction peak at 2θ value 27.64°, this can be attributed to the (002) diffraction planes of the graphite-like carbon nitride and correspond to the stacking inter planar peaks characteristic to aromatic systems. The second small angle peak at 13.02°, is indexed as (100) interlayer stacking. Conversely, the XRD pattern of KOH

treated G-C₃N₄ (at 730 °C for 2 min) exhibited a decrease in the intensity of peak at 2θ value 27.64° (Jiang et al. 2020). The most acceptable explanation of this matter is the partial decomposition of the network of G-C₃N₄ upon KOH treatment, resulting in the functionalization of graphitic carbon nitride surface with –OH, and NH_x groups (Jiang et al. 2020).

The surface functionalization of graphitic carbon nitride nanosheets was also evident in the XPS measurement. Additional file 1: Fig. S3A and B displays the XPS survey spectrum of G-C₃N₄ and T/G-C₃N₄ nanosheets. The results display an increase in the intensity of C1s peak and a decrease in the intensity of N 1s peak with a new peak attributed to O 1s in the T/G-C₃N₄ survey scan, further proving the introduction of more oxygen-containing functional groups on the graphitic carbon nitride surface after rapid KOH treatment at 730 °C for 2 min. Furthermore, the surface elements including C, N and O were detected (Additional file 1: Table S1). The C content of G-C₃N₄ (45.98%) was lower than T/G-C₃N₄

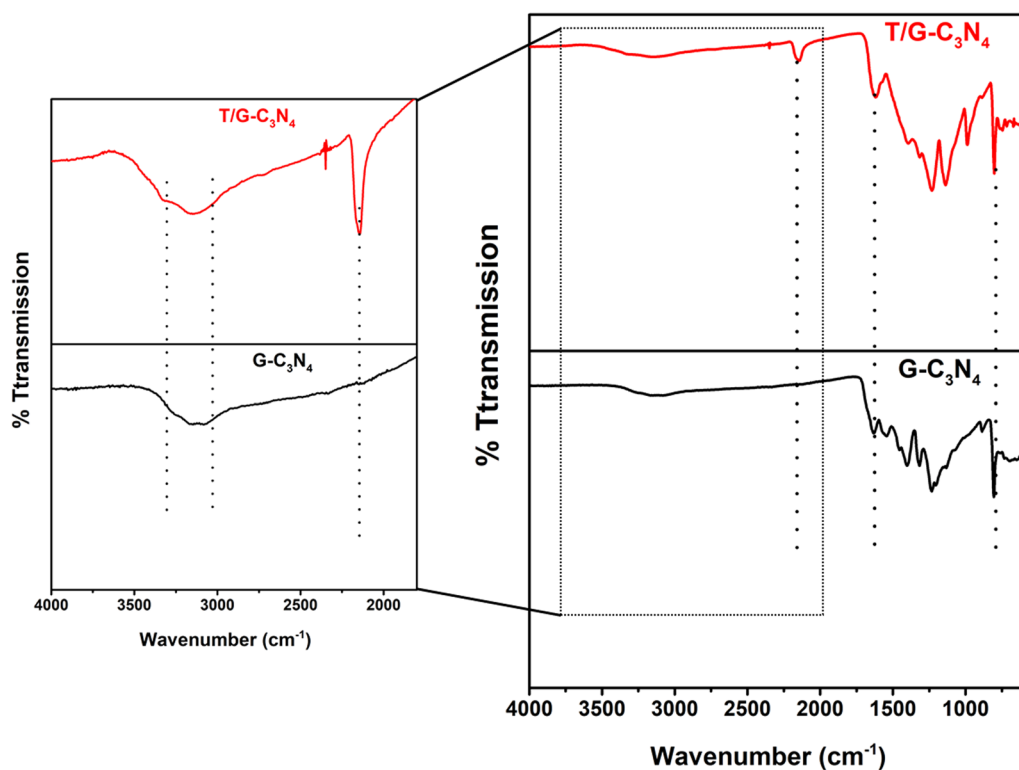


Fig. 2 FTIR spectra of G-C₃N₄, and T/G-C₃N₄ nanosheets

(58.23%) and the O content of T/G-C₃N₄ (11.55%) was higher than G-C₃N₄ (2.62%).

The grafting of the OH, O=CN, NH₂, and CN groups above the surface of T/G-C₃N₄ nanosheets, as described below, is further supported by detailed analyses of the XPS spectra of T/G-C₃N₄. The C 1s spectrum of G-C₃N₄ (Fig. 3A) is divided into three peaks with binding energies of 284.28 eV (C in -C=C-, -C-C- bonds), 287.4 eV (C in C-N-C bond), and 287.8 eV (C in C=N- of the triazine ring) (Qiao et al. 2015; Wei et al. 2018; Yu et al. 2017). However, the high resolution of C 1s spectrum related to T/G-C₃N₄ (Fig. 3B) can be divided into three peaks at 287.5 eV (C in N-C=O or -C=N-), 285.4 eV (C in CN or C-O bonds), 284.38 eV (C in -C=C- bond) (Qiao et al. 2015; Wei et al. 2018; Yu et al. 2017). The successful grafting of the OH and CN, N-C=O groups in T/G-C₃N₄ is also indicated by the N 1s (Fig. 3C) and O 1s (Fig. 3D). The N 1s spectrum can be divided into three peaks 398.3 eV (N in C-N=C of tri-s-triazine rings), 399.9 eV (N in N-(C)₃) of sp³-hybridized nitrogen in tri-s-triazine rings and 400.7 eV (N in -NH bonds of amine functional groups) (Qiao et al. 2015; Yu et al. 2017). These results revealed that the OH released via KOH treatment can uptake proton on the tri-s-triazine rings leading to the formation of amino and cyano groups. Additionally, The high resolution of O 1s spectrum (Fig. 3D) can be

divided into two peaks 532.18 eV (O in H₂O physically adsorbed onto graphitic carbon nitride sheets), 529.81 eV (O in -OH bonds), confirming the effect of KOH treatment on increasing the number of grafted OH groups on the surface of graphitic carbon nitride sheets (Wei et al. 2018). The FTIR and XPS spectra provide a convincing proof that the graphitic carbon nitride nanosheets were successfully functionalized after quick KOH treatment at 730 °C.

Figure 4 shows the SEM images of G-C₃N₄ (A and B) and T/g-C₃N₄ (C and D). As compared to that of pristine G-C₃N₄, SEM images of T/G-C₃N₄ display that graphitic carbon nitride sheets becomes smaller and thinner, as well as without surface agglomeration indicating the successful cracking and exfoliation of large graphitic carbon nitride sheets upon alkaline treatment with KOH at 730 °C for 2 min. This means that the number of available binding active sites on the surface of graphitic carbon nitride increased by KOH treatment at 730 °C for 2 min (Wang et al. 2020).

The UV-Vis absorption spectra of pure G-C₃N₄ and T/G-C₃N₄ in water are shown in Additional file 1: Fig. S4A. The charge transfer from a populated valence band of nitrogen atoms (2p orbitals) to a conduction band of carbon atoms (2p orbitals) of carbon nitride results in an absorption spectrum between 220 and 450 nm, as shown

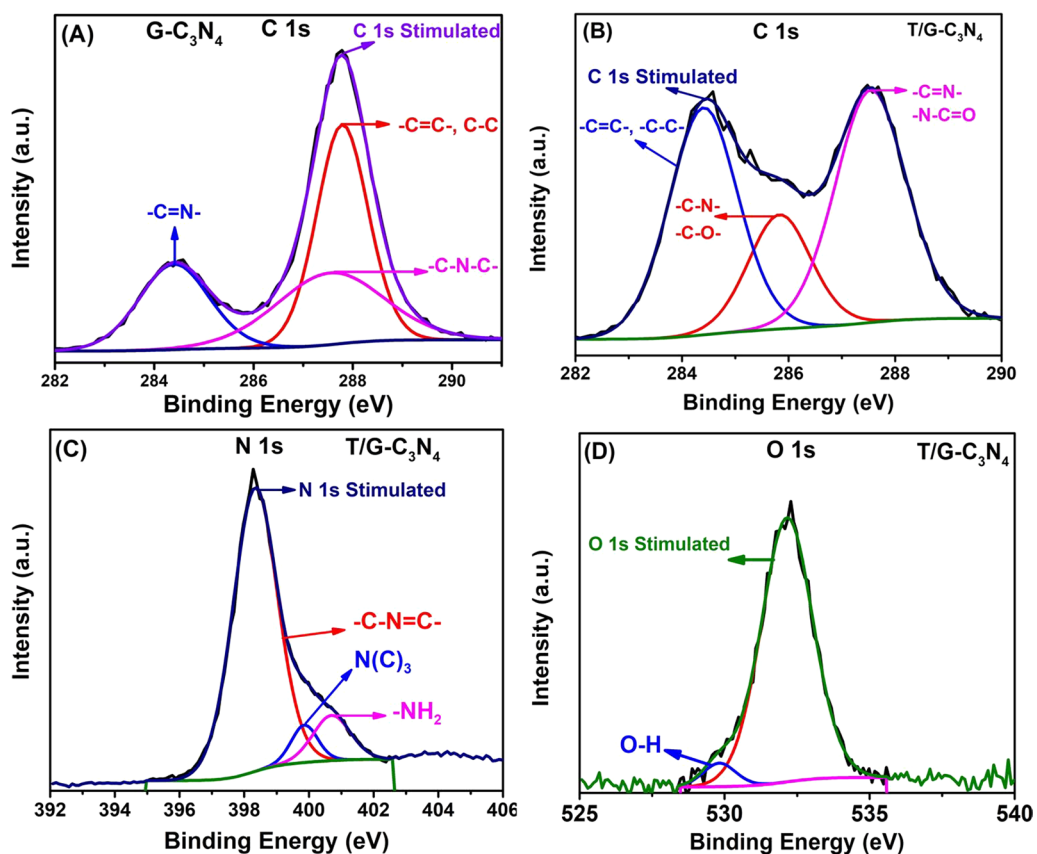


Fig. 3 XPS high resolution spectra of C1s in G-C₃N₄ (A), C1s in T/G-C₃N₄ (B), O 1s in T/G-C₃N₄ (C) and N 1s in T/G-C₃N₄ (D)

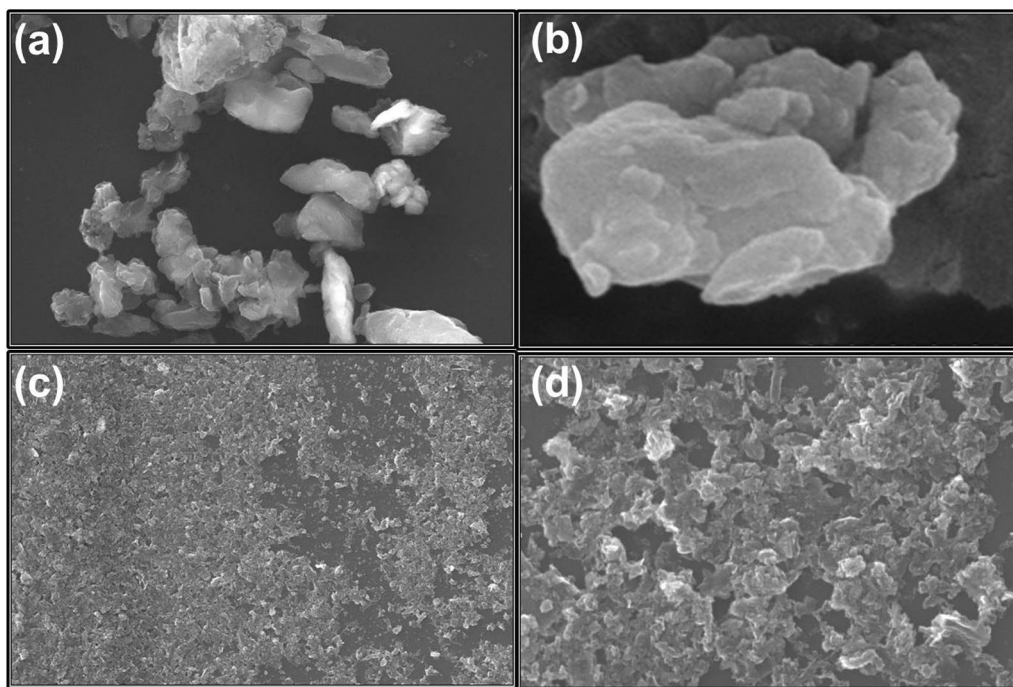


Fig. 4 SEM images of G-C₃N₄ (a, b), and T/G-C₃N₄ (c, d)

by the two spectra (Bakry et al. 2022). A peak at 320 nm assigned to $n-\pi^*$ transitions caused by the electron transfer from a nitrogen nonbonding orbital to an aromatic anti-bonding orbital (Awad et al. 2020). Additionally, the rapid KOH heat treatment can slightly weaken the connection between C and N in the “melon” structures. Therefore, the absorption band resulting from $n-\pi^*$ transition was reduced. Whereas the absorption band observed at 288 nm represented a $\pi-\pi^*$ transition of the C=N as polarizable sensing sites in the heptazine units (Awad et al. 2020; Bakry et al. 2022). The fluorescence emission spectrum of T/G-C₃N₄ is shown in Additional file 1: Fig. S4B. Wavelength was changed from (250–300 nm) to investigate the excitation dependent emission of the T/G-C₃N₄ as the maximum emission intensity of the T/G-C₃N₄ was attained at 377 nm ($\lambda_{\max}=290$ nm).

Fluorescence studies

Studying the effect of pH on the emission fluorescence intensity of T/G-C₃N₄ was investigated. It is well known that probes used in biological and environmental applications should have a wide pH viable range. Additional file 1: Fig. S5 illustrates how pH affects the T/G-C₃N₄ probe. The results revealed that T/G-C₃N₄ can be utilized as a probe across a wide pH range from pH 6 to pH 10 because these pH values have a little effect on the emission intensity of the probe, whereas this intensity decreases sharply in the pH range of 2–5. The T/G-C₃N₄ probe's long-term stability was also investigated. The T/G-C₃N₄ dispersion was kept in a brown flask and stored in dark at room temperature. The intensity of T/G-C₃N₄ has slightly changed, but not by more than 4.0%, despite being stored for more than 30 days.

To determine T/G-C₃N₄ capacity as a probe for Hg²⁺ detection. Figure 5A demonstrates how the introduction of the Hg²⁺ ion at pH 6 (phosphate buffer) significantly reduced the T/G-C₃N₄ fluorescence emission intensity, confirming that Hg²⁺ can efficiently quench the fluorescence of T/G-C₃N₄ nanosheets. The high tendency of mercury ions to form stable complexes with N-donors and the subsequent electron transfer from T/G-C₃N₄ to the complexed form with mercury can be used to explain the quenching of fluorescence emission caused by the Hg²⁺ ion (Afshani et al. 2017). Figure 5A showed that as Hg²⁺ concentration was increased from 0 to 3.0 ppm, the fluorescence emission intensity of T/G-C₃N₄ at 377 nm ($\lambda_{\max}=290$ nm) steadily reduced until it completely quenched at 3 ppm Hg²⁺. The increased affinity and fast chelating kinetics of Hg²⁺ with the NH₂, CN, C=N, and OH groups on the surface of alkali treated graphitic carbon nitride explained the high sensitivity of T/G-C₃N₄ towards the Hg²⁺ ions. Additionally, Hg²⁺ ions are willing to bind to the T/G-C₃N₄ surface, as it has many free

electrons. Typically, in T/G-C₃N₄, electrons get excited then transfer from the valence band (VB) to the conduction band (CB). Then, after the interactions between T/G-C₃N₄ and Hg²⁺, these excited electrons transfer from the CB of T/G-C₃N₄ to the LUMO of the cations. Consequently, the fluorescence is quenched as a result from the recombination of photo induced electron-holes (Azimi et al. 2019). Figure 5B displays a linear relationship between Hg²⁺ concentration and emission intensities, (I/I_0 is dependent on Hg²⁺ ion concentration; $R^2=0.9908$), where I and I_0 are the fluorescence intensities in the presence and absence of Hg²⁺, respectively. The T/G-C₃N₄ is appropriate as a sensitive detection probe for mercury ions, as the detection limit is suggested to be 27 nM. The constructed T/G-C₃N₄ probe is thought to be a promising probe for detecting Hg²⁺ in various water samples since it has a wide linear range and good linear relation when compared to previously reported probes in the literature.

Time-dependent fluorescence quenching of T/G-C₃N₄-Hg²⁺ solution was investigated. The fluorescence quenching increased with increasing reaction times between Hg²⁺ and T/G-C₃N₄, as seen in Additional file 1: Fig. S6. According to Additional file 1: Fig. S6, the reaction between T/G-C₃N₄ and Hg²⁺ takes 5 min to complete.

Selectivity is a crucial factor in determining the effectiveness of T/G-C₃N₄ as a probe for Hg²⁺ ions. In order to investigate the selectivity of T/G-C₃N₄ probe towards Hg²⁺, we checked the change in fluorescence emission intensity in the presence of other metal ions under the same conditions. As shown in Fig. 5C, The fluorescence emission of T/G-C₃N₄ quenched by the addition of Hg²⁺ only (about 100% quenching happened after the addition of 3.0 ppm Hg²⁺ in phosphate buffer pH 6); no significant quenching effect was seen after the addition of other metal ions (Na⁺, Ag⁺, Ca²⁺, K⁺, Mg²⁺, Fe²⁺, Fe³⁺, Ni²⁺, Pb²⁺, Co²⁺, Cd²⁺, Zn²⁺, and Cu²⁺). Due to the unshared electrons of the nitrogen atoms in the heptazine unit of T/G-C₃N₄, Hg²⁺ has a stronger tendency to coordinate with it (Awad et al. 2020; Patel and Kailasa 2022). Mercury ions can effectively quench the fluorescence intensity of T/G-C₃N₄ via electron transfer mechanisms.

The influence of other metal ions (interfering ions) that coexist with mercury ions in real samples on the fluorescence emission intensity of T/G-C₃N₄ probe was tested and the results are in Fig. 5D. The results revealed that the emission intensity of T/G-C₃N₄ remained unchanged in the presence of other metal ions, indicating that mercury ions have a higher affinity for binding with the OH, NH_x groups and heptazine units on the surface of T/G-C₃N₄ than other metal ions (Awad et al. 2020; Azimi et al. 2019; El-Wakil et al.

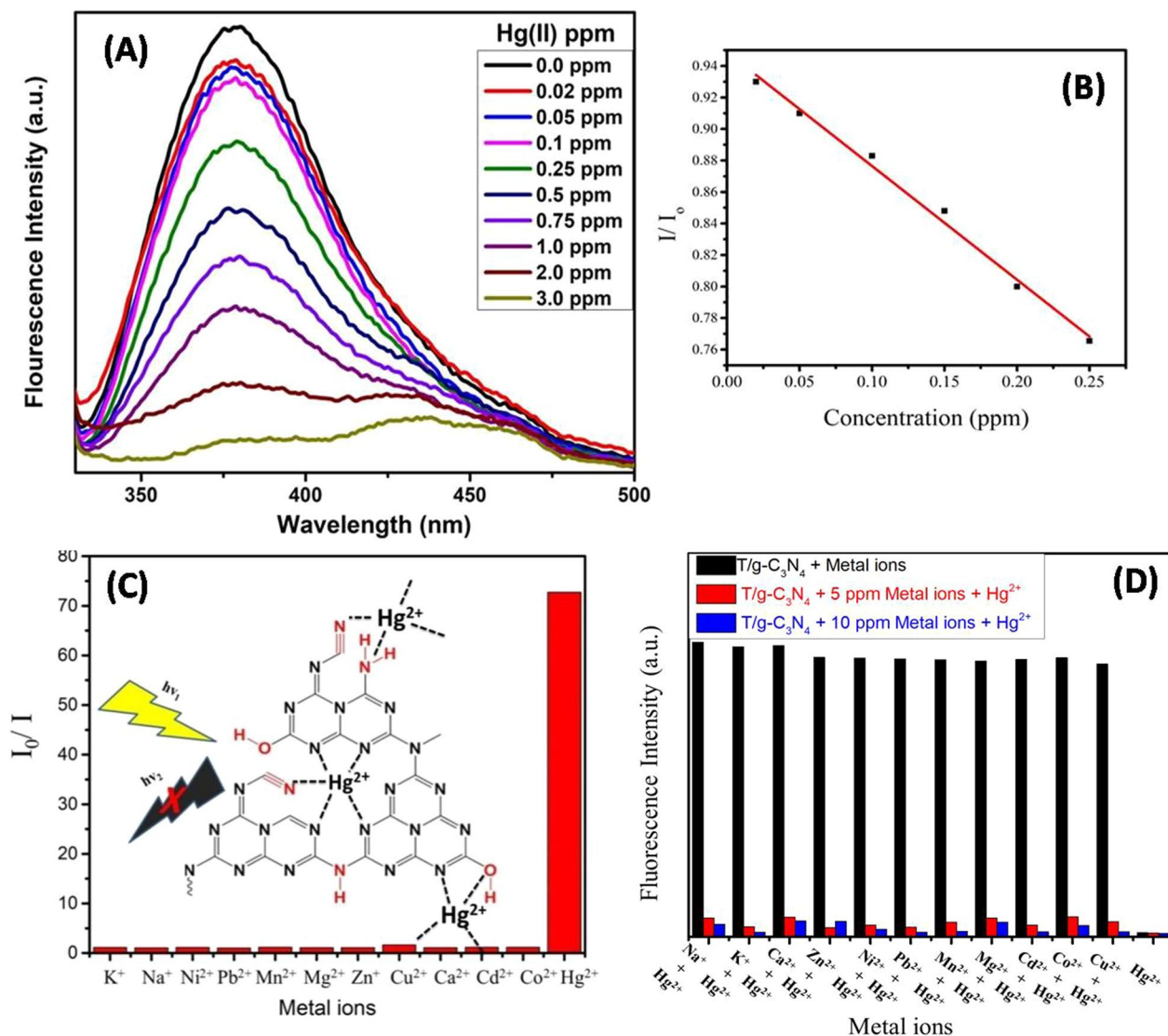


Fig. 5 **A** Fluorescence emission spectra of T/G-C₃N₄ in 0.01 M phosphate buffer (pH=6.0), with Hg²⁺ at various concentrations (0–3.0 ppm), T/G-C₃N₄ at 3.0 mg/L, reaction time at 5 min, and excitation at 290.0 nm. **B** The linear relationship between Hg²⁺ concentration and emission intensities. **C** Selectivity of T/G-C₃N₄ (3.0 mg/L) for various metal ions at a concentration of 3.0 ppm (where *I* and *I*₀ represent the fluorescence intensities of T/G-C₃N₄ in the presence and absence of metal ions, respectively) and the red colored atoms refer to the new bonds (OH, NH₂, NH_x, and CN groups) formed onto the surface of G-C₃N₄ due to the partial deprotonation of melon units after thermal alkali treatment. **D** Fluorescence responses of T/G-C₃N₄ to competing metal ions (5.0 mg/L) black bars to Hg²⁺ ions (3.0 ppm, red and blue bars), in 0.01 M phosphate buffer (pH=6.0), T/G-C₃N₄= (3.0 mg/L), excitation at 290 nm)

2022). The capacity of T/G-C₃N₄ to bind with several metal ions, including Hg²⁺ ions, Na⁺, Ag⁺, K⁺, Ca²⁺, Fe²⁺, Fe³⁺, Mg²⁺, Ni²⁺, Co²⁺, Pb²⁺, Cd²⁺, Zn²⁺, and Cu²⁺, presented an elective response towards mercury ions. The addition of Hg²⁺ to T/G-C₃N₄ probes containing different concentrations of interfering ions caused a considerable change, as seen in Fig. 5D, demonstrating that the T/G-C₃N₄ has a higher binding affinity for Hg²⁺ than other metal ions at pH=6. All of

the obtained results revealed that T/G-C₃N₄ is highly selective and sensitive for the detection of mercury ions in aqueous media.

Actual sample analysis

To check the usability of the proposed nanoprobe, it was important to use the T/G-C₃N₄ probes in detecting and quantifying Hg²⁺ ions in some food samples. The influence of adding solutions made up from commercially

Table 1 Detection of Hg²⁺ ions in tuna fish and mackerel fish using ICP-AES and T/G-C₃N₄ probe

Fish sample	[Hg ²⁺] by ICP-AES (μM)	[Hg ²⁺] by T/G-C ₃ N ₄ probe (μM)
Tuna fish	0.41 ± 0.03 ^a	0.5 ± 0.03 ^a
Mackerel fish	0.65 ± 0.02 ^a	0.70 ± 0.02 ^a

^a Standard deviation

available mackerel and tuna fish samples (collected from local market) on the emission profile of the T/G-C₃N₄ was investigated (Additional file 1: Fig. S7). Laboratory solutions of mackerel and tuna fish were made, as mentioned before in the experimental part, and the appropriate amounts of each solution were added to the T/G-C₃N₄ solution. The quenching in the fluorescence emission intensities of T/G-C₃N₄ was then measured, and this information was used to determine the concentration of Hg²⁺ ions in the initial unknown solutions. Table 1 shows the results obtained using T/G-C₃N₄ probe and ICP-AES method. The obtained data confirm that the prepared T/G-C₃N₄ can be used as a selective Hg²⁺ probe in representative environmental samples.

Comparison of detection limits

A comparison to the previously reported probes in the literature (Additional file 1) has been made to illustrate the remarkable sensitivity and selectivity of the developed probe, the relevant data are presented in Additional file 1: Table S2. Among the different fluorescent probes, the developed environmental probe exhibited a good linear relation and wide linear range. Consequently, T/g-C₃N₄ is recognized as a sensitive, selective, cost effective, and useful platform for detection of Hg²⁺ in water samples.

Conclusions

In conclusion, we have demonstrated the viability of employing graphitic carbon nitride nano sheets functionalized with -OH and -NH_x groups through a rapid KOH heat treatment method as a highly efficient probe for Hg²⁺ detection. FTIR, UV-Vis, XRD, XPS, and fluorescence spectra were used to analyze the surface morphology and structure of the T/G-C₃N₄. Based on the quenching effect, the T/G-C₃N₄ showed a linear response with Hg²⁺ over concentration range 0–1.25 × 10³ nM; the detection limit was 27 nM. T/G-C₃N₄ probe displayed remarkable sensitivity and selectivity for Hg²⁺ owing to the presence of the NH₂, CN, C=N, and OH groups of T/G-C₃N₄ nanosheets which have a high binding affinity with Hg²⁺. The developed T/G-C₃N₄ probe, on the other hand, exhibits strong anti-interference performance against 11 different types of coexisting cations. The prepared T/G-C₃N₄ probe also

displayed a wide pH viable range, remarkable photo stability, and outstanding long-term fluorescence stability (> 30 days). Moreover, the analysis of real samples showed that our proposed T/G-C₃N₄ probe had a good potential for measuring Hg²⁺ concentration in food samples (tuna and mackerel fish). These findings demonstrated that the developed environmental probe is a low-cost, effective, and useful platform for selective and rapid monitoring of mercury ions in the environment.

Supplementary Information

The online version contains supplementary material available at <https://doi.org/10.1186/s40543-023-00379-0>.

Additional file 1: S1. Chemicals and materials. **S2.** Instruments. **Fig. S1.** Electron density charge distributions of T/G-C₃N₄. **Fig. S2.** XRD patterns of G-C₃N₄ and T/G-C₃N₄. **Fig. S3.** XPS survey spectra of G-C₃N₄ (A) and T/G-C₃N₄ (B). **Table S1.** The elemental composition of G-C₃N₄ and T/G-C₃N₄ from XPS analysis. **Fig. S4.** A UV-Vis spectra of G-C₃N₄ and T/G-C₃N₄. **B** Fluorescence spectra of T/G-C₃N₄ at various excitation wavelengths. **Fig. S5.** The effect of pH on the fluorescence intensities of T/G-C₃N₄. **Fig. S6.** Time-dependent fluorescence quenching of T/G-C₃N₄. **Fig. S7.** Fluorescence intensity emission of T/G-C₃N₄ up on addition of definite volume of Tuna fish and mackerel fish. **Table S2.** Comparison between fluorescent probes for Hg²⁺ and this work.

Acknowledgements

Not applicable.

Author contributions

YGAE-R and FSA: synthesis, writing original draft, data analysis, editing, proofreading, and manuscript handling. EAG: computational approaches, data analysis, and writing the original draft. HL: supervision, initial corrections, and comments. OE-A, FKA and EAA: graphical plots, data analysis. All authors read and approved the final form of the manuscript.

Funding

Open access funding provided by The Science, Technology and Innovation Funding Authority (STDF) in cooperation with The Egyptian Knowledge Bank (EKB).

Availability of data and materials

Not applicable.

Declarations

Competing interests

The authors declare that they have no competing interests.

Author details

¹Chemistry Department, Faculty of Science, Mansoura University, Mansoura 23768, Egypt. ²Department of Chemistry, Faculty of Science, Imam Mohammad Ibn Saud Islamic University, P.O. Box 90950, Riyadh 11623, Saudi Arabia. ³Department of Chemical and Biological Engineering, University at Buffalo, The State University of New York, Buffalo, NY 14260, USA. ⁴Department, Faculty of Science, Benha University, Benha, Egypt.

Received: 12 December 2022 Accepted: 15 February 2023

Published online: 01 March 2023

References

Abdallah A, Ghaith EA, Mortada WI, Molouk AFS. Electrochemical sensing of sodium dehydroacetate in preserved strawberries based on in situ

- pyrrole electropolymerization at modified carbon paste electrodes. *Food Chem.* 2022;401:134058.
- Afshani J, Badieli A, Karimi M, Lashgari N, Mohammadi Ziarani G. A Schiff base-grafted nanoporous silica material as a reversible optical probe for Hg²⁺ ion in water. *Appl Organometal Chem.* 2017;31(12):e3856.
- Al-Assy WH, El-Askalany AMH, Mostafa MM. Structural comparative studies on new MnII, CrIII and RuIII complexes derived from 2, 4, 6-tri-(2-pyridyl)-1, 3, 5-triazine (TPTZ). *Spectrochim Acta Part A Mol Biomol Spectrosc.* 2013;116:401–7.
- Anderson M, McDonnell J, Ximing C, Cline S, Balance W, Rockstrom J, et al. The challenge of micropollutants in aquatic systems. *Science.* 2006;313(August):1072–7.
- Awad FS, AbouZeid KM, El-Maaty WMA, El-Wakil AM, El-Shall MS. Efficient removal of heavy metals from polluted water with high selectivity for mercury (II) by 2-imino-4-thiobiuret–partially reduced graphene oxide (IT-PRGO). *ACS Appl Mater Interfaces.* 2017;9(39):34230–42.
- Awad FS, AbouZied KM, Bakry AM, Abou El-Maaty WM, El-Wakil AM, El-Shall MS. Highly fluorescent hematoporphyrin modified graphene oxide for selective detection of copper ions in aqueous solutions. *Anal Chim Acta.* 2020;1140:111–21.
- Azimi EB, Badieli A, Jafari M, Dehkordi AB, Ghasemi JB, Ziarani GM. Boron-doped graphitic carbon nitride as a novel fluorescent probe for mercury (ii) and iron (iii): a circuit logic gate mimic. *New J Chem.* 2019;43(30):12087–93.
- Bakry AM, Alamier WM, El-Shall MS, Awad FS. Facile synthesis of amorphous zirconium phosphate graphitic carbon nitride composite and its high performance for photocatalytic degradation of indigo carmine dye in water. *J Mater Res Technol.* 2022;20:1456–69.
- Cárdenas A, Vázquez A, Obregón S, Ruiz-Gómez M, Rodríguez-González V. New insights into the fluorescent sensing of Fe³⁺ ions by g-C₃N₄ prepared from different precursors. *Mater Res Bull.* 2021;142:111385.
- El-Wakil AM, Waly SM, Abou El-Maaty WM, Waly MM, Yilmaz M, Awad FS. Triazine-based functionalized activated carbon prepared from water hyacinth for the removal of Hg²⁺, Pb²⁺, and Cd²⁺ ions from water. *ACS Omega.* 2022;7(7):6058–69.
- Erdemir S, Oguz M, Malkondu S. A NIR fluorescent sensor based on thiazoline-isophorone with low cytotoxicity in living cells for Hg²⁺ detection through ICT associated hydrogen bonding effect. *Anal Chim Acta.* 2022;1192:339353.
- Ghaith EA, Zoorob HH, Ibrahim ME, Sawamura M, Hamama WS. Convenient synthesis of binary and fused pyrazole ring systems: accredited by molecular modeling and biological evaluation. *ChemistrySelect.* 2020;5(47):14917–23.
- Jiang K, Zhu L, Wang Z, Liu K, Li H, Hu J, et al. Plasma-treatment induced H₂O dissociation for the enhancement of photocatalytic CO₂ reduction to CH₄ over graphitic carbon nitride. *Appl Surf Sci.* 2020;508:145173.
- Krabbenhoft DP, Sunderland EM. Global change and mercury. *Science.* 2013;341(6153):1457–8.
- Li X, Zhang X, Ma H, Wu D, Zhang Y, Du B, et al. Cathodic electrochemiluminescence immunosensor based on nanocomposites of semiconductor carboxylated g-C₃N₄ and graphene for the ultrasensitive detection of squamous cell carcinoma antigen. *Biosens Bioelectron.* 2014;55:330–6.
- Li Y, Xu H, Ouyang S, Lu D, Wang X, Wang D, et al. In situ surface alkalized gC₃N₄ toward enhancement of photocatalytic H₂ evolution under visible-light irradiation. *J Mater Chem A.* 2016;4(8):2943–50.
- Mortada W, Kenawy I, Abou El-Reash Y, Mousa A. Microwave assisted modification of cellulose by gallic acid and its application for removal of aluminium from real samples. *Int J Biol Macromol.* 2017;101:490–501.
- Mortazavi S, Mortazavi G, Paknahad M. A review on the distribution of Hg in the environment and its human health impacts. *J Hazard Mater.* 2016;310:278–9.
- Patel MR, Kailasa SK. Carbon nitride nanomaterials: properties, synthetic approaches and new insights in fluorescence spectrometry for assaying of metal ions, organic and biomolecules. *ChemistrySelect.* 2022;7(27):e202201849.
- Pica M. Treatment of wastewaters with zirconium phosphate based materials: a review on efficient systems for the removal of heavy metal and dye water pollutants. *Molecules.* 2021;26(8):2392.
- Premkumar M, Thiruvengadaravi K, Senthil Kumar P, Nandagopal J, Sivasenan S. Eco-friendly treatment strategies for wastewater containing dyes and heavy metals. In: Gupta T, Agarwal AK, Agarwal RA, Labhsetwar NK, editors. *Environmental contaminants*. Berlin: Springer; 2018. p. 317–60.
- Qiao F, Wang J, Ai S, Li L. As a new peroxidase mimetics: the synthesis of selenium doped graphitic carbon nitride nanosheets and applications on colorimetric detection of H₂O₂ and xanthine. *Sens Actuators B Chem.* 2015;216:418–27.
- Ramki K, Venkatesh N, Sathiyam G, Thangamuthu R, Sakthivel P. A comprehensive review on the reasons behind low power conversion efficiency of dibenzo derivatives based donors in bulk heterojunction organic solar cells. *Org Electron.* 2019;73:182–204.
- Rasheed T, Nabeel F, Li C, Bilal M. Rhodamine-assisted fluorescent strategy for the sensitive and selective in-field mapping of environmental pollutant Hg (II) with potential bioimaging. *J Lumin.* 2019;208:519–26.
- Romanovskiy KA, Bolshov MA, Münz AV, Temerdashev ZA, Burylin MY, Sirota KA. A novel photochemical vapor generator for ICP-MS determination of As, Bi, Hg, Sb, Se and Te. *Talanta.* 2018;187:370–8.
- Sun X-J, Liu T-T, Li N-N, Zeng S, Xing Z-Y. A novel dual-function probe for recognition of Zn²⁺ and Al³⁺ and its application in real samples. *Spectrochim Acta Part A Mol Biomol Spectrosc.* 2020;228:117786.
- Tian Z-N, Wu D-Q, Sun X-J, Liu T-T, Xing Z-Y. A benzothiazole-based fluorescent probe for ratiometric detection of Al³⁺ and its application in water samples and cell imaging. *Int J Mol Sci.* 2019;20(23):5993.
- Wang Y-W, Wang L, An F, Xu H, Yin Z, Tang S, et al. Graphitic carbon nitride supported platinum nanocomposites for rapid and sensitive colorimetric detection of mercury ions. *Anal Chim Acta.* 2017;980:72–8.
- Wang N, Wang R, Tu Y, Pu S, Liu G. A novel fluorescence “turn-on” sensor based on a photochromic diarylethene for the selective detection of Al (III). *Spectrochim Acta Part A Mol Biomol Spectrosc.* 2018a;196:303–10.
- Wang H, Lu Q, Li M, Li H, Liu Y, Li H, et al. Electrochemically prepared oxygen and sulfur co-doped graphitic carbon nitride quantum dots for fluorescence determination of copper and silver ions and biothiols. *Anal Chim Acta.* 2018b;1027:121–9.
- Wang Q, Zhang L, Guo Y, Shen M, Wang M, Li B, et al. Multifunctional 2D porous g-C₃N₄ nanosheets hybridized with 3D hierarchical TiO₂ microflowers for selective dye adsorption, antibiotic degradation and CO₂ reduction. *Chem Eng J.* 2020;396:125347.
- Wang X, Hu C, Wang X, Luo Z, Zhen S, Zhan L, et al. Facile synthesis of dual-ligand terbium-organic gels as ratiometric fluorescence probes for efficient mercury detection. *J Hazard Mater.* 2022;436:129080.
- Wei Z, Liu M, Zhang Z, Yao W, Tan H, Zhu Y. Efficient visible-light-driven selective oxygen reduction to hydrogen peroxide by oxygen-enriched graphitic carbon nitride polymers. *Energy Environ Sci.* 2018;11(9):2581–9.
- Xie F, Song Z-Y, Yang M, Duan W-C, Quan Y-N, Huang X-J, et al. Enhanced electrochemical sensing performance for trace Hg (II) by high activity of Co³⁺ on Co₃O₄-NP/N-RGO surface. *Anal Chim Acta.* 2022;1200:339607.
- Xu Y, Niu X, Zhang H, Xu L, Zhao S, Chen H, et al. Switch-on fluorescence sensing of glutathione in food samples based on a graphitic carbon nitride quantum dot (g-CNQD)-Hg²⁺ chemosensor. *J Agric Food Chem.* 2015;63(6):1747–55.
- Yang P, Wang L, Zhuzhang H, Wang R, Titirici M-M, Wang X. Photocarving nitrogen vacancies in a polymeric carbon nitride for metal-free oxygen synthesis. *Appl Catal B Environ.* 2019;256:117794.
- Yin M, Wan Y, Li S, Zhao X, Zhang W, Zhang Y, et al. Carbon nitride-doped melamine-silver adsorbents with peroxidase-like catalysis and visible-light photocatalysis: colorimetric detection and detoxification removal of total mercury. *J Hazard Mater.* 2021;408:124978.
- Yu H, Shi R, Zhao Y, Bian T, Zhao Y, Zhou C, et al. Alkali-assisted synthesis of nitrogen deficient graphitic carbon nitride with tunable band structures for efficient visible-light-driven hydrogen evolution. *Adv Mater.* 2017;29(16):1605148.
- Zhang J, Yu S-H. Highly photoluminescent silicon nanocrystals for rapid, label-free and recyclable detection of mercuric ions. *Nanoscale.* 2014;6(8):4096–101.
- Zhang G, Lin L, Li G, Zhang Y, Savateev A, Zafeiratos S, et al. Ionothermal synthesis of triazine–heptazine-based copolymers with apparent quantum yields of 60% at 420 nm for solar hydrogen production from “sea water.” *Angew Chem.* 2018;130(30):9516–20.

Publisher's Note

Springer Nature remains neutral with regard to jurisdictional claims in published maps and institutional affiliations.